Origin of periodic rippling during chemical vapor deposition growth of carbon nanotube forests

Vinten, P.; Bond, J.; Marshall, P.; Lefebvre, J.; Finnie, P.

Publisher's version / Version de l'éditeur:
https://doi.org/10.1016/j.carbon.2011.02.017
Carbon, 49, 15, pp. 4972-4981, 2011-02-13

CARBON 49 (2011) 4972–4981

available at www.sciencedirect.com

ScienceDirect

journal homepage: www.elsevier.com/locate/carbon

Origin of periodic rippling during chemical vapor deposition growth of carbon nanotube forests

P. Vinten [a,b], J. Bond [a,b], P. Marshall [a], J. Lefebvre [a], P. Finnie [a,b,*]

[a] Institute for Microstructural Sciences, National Research Council Canada, Building M-50, 1200 Montreal Road, Ottawa, ON, Canada K1A 0R6

[b] Department of Physics, University of Ottawa, 150 Louis Pasteur, Ottawa, ON, Canada K1N 6N5

ARTICLE INFO

Article history:
Received 25 November 2010
Accepted 8 February 2011
Available online 13 February 2011

ABSTRACT

Carbon nanotube forests are arrays of roughly vertically aligned nanotubes. Under certain growth conditions, these forests can show a growth instability that gives rise to periodic ripples that are coherent over a forest-sized scale. Previously, we showed that the uniformity and synchronization of the ripples is sufficient for them to behave as diffraction gratings for visible light. Here, we identify the conditions that reproducibly promote the formation of these ripples. We investigate the formation mechanism via *ex situ* scanning electron microscopy and *in situ* optical imaging. While the rippling amplitude varies appreciably, the rippling wavelength varies very little and can be estimated from simple mechanical considerations. We provide evidence that the rippling is a consequence of cohesive interactions between nanotubes and the build up of strain, driven by a non-uniform growth rate. The origin of the non-uniform growth rate is explained.

1. Introduction

The growth of vertically aligned carbon nanotube forests is studied extensively because it represents one of the highest yield methods of nanotube growth. Originally observed in multi-walled carbon nanotube (MWCNT) samples, vertically aligned single-walled carbon nanotube (SWCNT) forests are now the focus of much attention. Over large length scales, the nanotubes in forests appear densely packed and, on average, very straight and well aligned. However, closer analysis via scanning electron microscopy (SEM) reveals that, on the micrometer scale, forests are mostly empty space filled with individual nanotubes and bundles of nanotubes that are far from straight, and instead meander back and forth in a seemingly random and disordered manner. Under certain growth conditions, the meandering becomes highly ordered, coherent, and synchronized over lengths of hundreds of μm such that the sidewalls of the forest have a rippling pattern on them. Previous reports of ripples on as-grown forests, such as in the present report, include ripples on forests grown with externally applied forces *in situ* [1], wandering nanotubes in forests due to specific catalyst pretreatment and preparation methods [2–5], ripples near the base of tall forests [6,7], and ripples due to a temperature non-uniformity in micrometer scale local heating [8]. A similar rippling pattern can also occur on forests (composed of initially straight nanotubes) that are intentionally subjected to externally applied mechanical compression *ex situ* [9–11]. The interactions between nanotubes have previously been shown to be important for forest morphology [6–8,12–19], and will be considered here.

In the present report, the forests are not compressed by external forces. The rippled nanotubes self-assemble during chemical vapour deposition (CVD) growth of the forests without any intentional special catalyst preparation or pretreatment, and are, most importantly, entirely reproducible. Remarkably, the ripples we obtain are sufficiently regular over

* *Corresponding author:* Address: Institute for Microstructural Sciences, National Research Council Canada, Building M-50, 1200 Montreal Road, Ottawa, ON, Canada K1A 0R6.
E-mail address: Paul.Finnie@nrc-cnrc.gc.ca (P. Finnie).
0008-6223/$ - see front matter
doi:10.1016/j.carbon.2011.02.017

a large enough area that they produce an easily observed optical effect: iridescence caused by the diffraction of visible light via a surface grating effect [20]. This iridescence provides a means to observe the ripples optically since they are too small for direct observation with visible light. In particular, it allows us to observe the ripples *in situ* and thus provides valuable clues to the nature of the formation mechanism responsible for these ripples. We identify the reactor conditions that promote the formation of ripples. Using *in situ* observations as well as *ex situ* SEM observations, we support a formation mechanism: the ripples are a growth instability caused by the build-up of strain within the forest as it grows due to a difference in growth rate between different nanotubes in the forest.

2. Experimental procedures

Samples were grown by water-assisted [21] CVD using acetylene as the carbon source [22–25], and alumina/cobalt thin films as the catalyst. We used a cold-walled CVD reactor, operated at atmospheric pressure, as described in our previous reports [12,26], with additional details given in [27,28]. The carbon source was supplied as dilute acetylene gas (0.1% C_2H_2, 99.9% Ar), assisted by hydrogen (2% H_2, 98% Ar) and water vapour obtained by passing pure Ar through a bubbler. Samples were ~ 0.3 cm^2 square pieces of 0.5 mm thick Si with 1 μm thermal SiO_2, and catalyst layers of nominally 250 nm Al_2O_3 and 0.8 nm Co deposited by e-beam evaporation through a shadow mask to produce 100 μm to 800 μm diameter circles in evenly spaced patterns. Some samples were also prepared using photolithography, but they are not presented in detail here. Forests grown under this range of conditions are expected to consist of a mixture of MWCNTs and SWCNTs [12].

In the present report, we vary the temperature and the source gas flow rate (see Appendix for procedural details). Unless otherwise stated, all forest growth self-terminated without external intervention such as stopping the flow of the carbon source. No external forces are applied to the forests during growth or after growth. *In situ* optical images and videos were acquired through the large glass window in the reactor using a long focal length optical microscope and digital camera at a glancing angle of ~5° to the substrate. *Ex situ* optical images and videos were acquired using the same microscope and camera in a different configuration. SEM images were obtained *ex situ* using a Hitachi S-4700 field emission SEM.

3. Results

Terminal forest heights H_t for the rippled forests varied from ~200 μm to ~500 μm for the 100 μm diameter forests and were ~1 mm for the 700 and 800 μm diameter forests. Maximum forest height, top surface concavity, and curvature of the sidewalls all occurred around 760 °C and 180 sccm source gas flow rate. Ripples form reproducibly on forests grown in the temperature range 730 °C < T < 800 °C at a source gas (C_2H_2) flow rate of 180 sccm, with the most prominent ripples (largest amplitudes) appearing around 760 °C. For forests grown at temperatures progressively further from 760 °C, the height, concavity, and curvature of the sidewalls all decreased, while the ripples simultaneously disappeared (their amplitude vanished). Outside of the above temperature range no rippling occurred; the top surfaces of the forests are flat and the sidewalls are smooth and vertical.

A similar trend was observed for the C_2H_2 flow rate dependence. Rippling occurred reproducibly for source gas flow rates (other gas flow rates fixed) between 100 sccm and 220 sccm at a growth temperature of 760 °C. The most prominent ripples occurred around 180 sccm: the same flow rate as the maximum forest height, concavity, and curvature of the sidewalls. At gas flow rates progressively further from 180 sccm, the height, concavity, and curvature of the sidewalls all decreased, while at the same time the ripples disappeared by diminishing amplitudes. Outside of the above flow rate range there are no ripples, the top surfaces of the forests are flat, and the sidewalls are smooth and vertical. Unlike the amplitude, the wavelength of the ripples did not vary much or show a clear trend with any change in the growth parameters.

The smaller diameter forests (100 μm) had ripples over most of the temperature and flow rate ranges analyzed, while the larger diameter forests (700 μm) had ripples only over a narrow temperature and flow rate range centered on 760 °C and 180 sccm. This suggests that there is a dependence on catalyst island size.

The rippling on the forests' sidewalls is synchronized over length scales similar to the size of the forest (see Fig. 1a). The rippling is characterized by smooth consistent curves without any sharp kinks or bends. For any given nanotube, the rippling occurs in a plane, thus they are not helixes such as those observed in other systems [29]. The ripples generally encircle the entire forest (Fig. 1a) from near the top on the curved portion of the sidewalls (Fig. 1b) and down the vertical sidewalls (Fig. 1c–d) where the amplitude slowly fades to zero (Fig. 1e–f) before reaching the base of the forest, where the nanotubes appear straight. In some previous reports, the ripples were observed to form only at the base of the forest [6,7]. Here, the ripples extend for a significant portion of the forest height, as seen in an earlier report [8]. Furthermore, all nanotubes on the forests' sidewalls participate in the rippling; no straight nanotubes are visible, in contrast to several other previous studies [2,3].

The ripples have a clearly defined and measurable wavelength and amplitude (see Fig. 2a for an example). The rippling amplitude was measured using SEM by looking tangentially to the circular cross section of the cylindrical forests. This shows the wave-like profile of the ripples, as shown in the example in Fig. 2a. The amplitude can then be simply measured as the height of the wave-like profile. From analyzing many forests, the amplitude is observed to vary from one forest to another, ranging from as large as ~1 μm to as small as zero. Although the rippling amplitude decreases gradually from the top of any given forest to the bottom, the variation is slow enough that it appears approximately constant (extremely slowly varying) over short distances of several tens of μm (see Fig. 2a).

The wavelength can be measured in the same way as the amplitude, though most wavelength measurements were taken using SEM looking normally toward the rippled

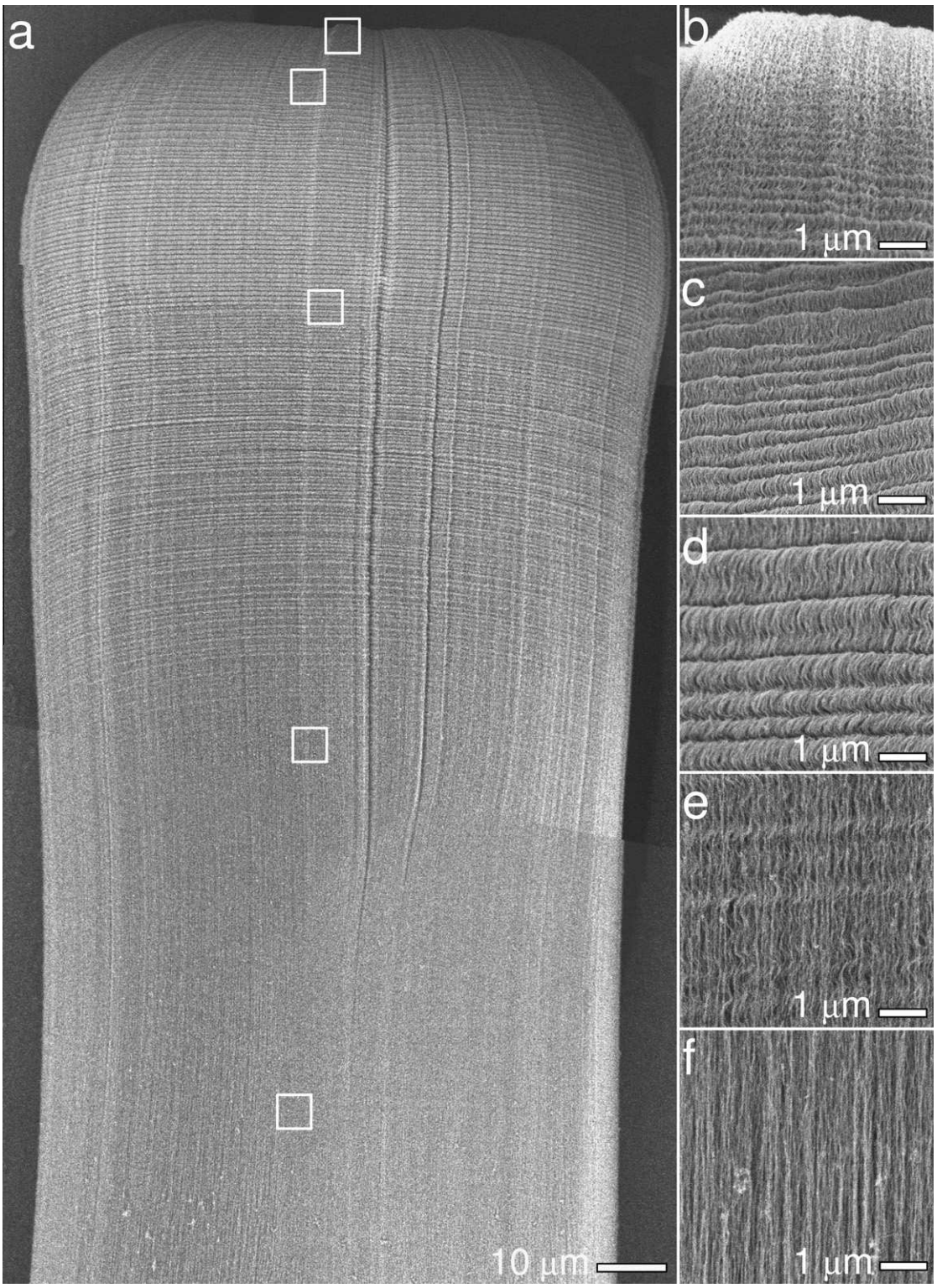

Fig. 1 – SEM images of rippled forest. (a) Top part of forest (~350 μm tall) grown on a 100 μm diameter catalyst island. This image was constructed from several individual SEM images. (b–f) Close-ups of indicated areas in (a). The ripples in (b) appear to have a short wavelength because the forest is curving away from the plane of view. This forest was grown at 730 °C using 180 sccm C_2H_2 flow rate.

sidewalls, similar to Fig. 3c. For such wavelength measurements, a high contrast between the peaks and valleys of the rippling pattern is more important than a high resolution that can distinguish the individual nanotubes. From analyzing many forests, the wavelength is observed to vary between ~300 nm and ~1 μm. This length is similar to the length scale

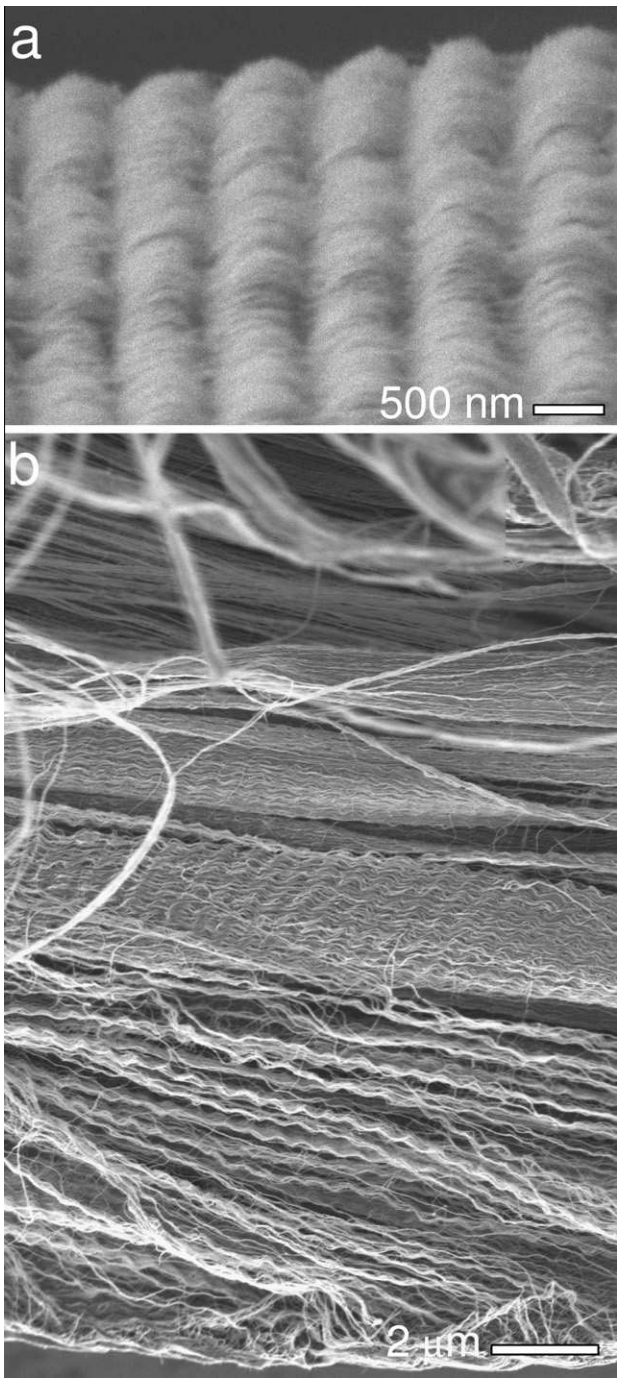

Fig. 2 – SEM images of ripples on 100 μm diameter forests. (a) Wavelength and amplitude seen looking tangential to the forest circumference (at a glancing angle to the outer wall of the forest). (b) Forest (horizontal orientation) split open along its length, showing the amplitude decreasing to zero toward the center of the forest. The view is along the forest radius, looking into the split, toward the center of the forest. This image was constructed from several individual SEM images. These forests were grown at 730 °C and 760 °C respectively, using 180 sccm C_2H_2 flow rate.

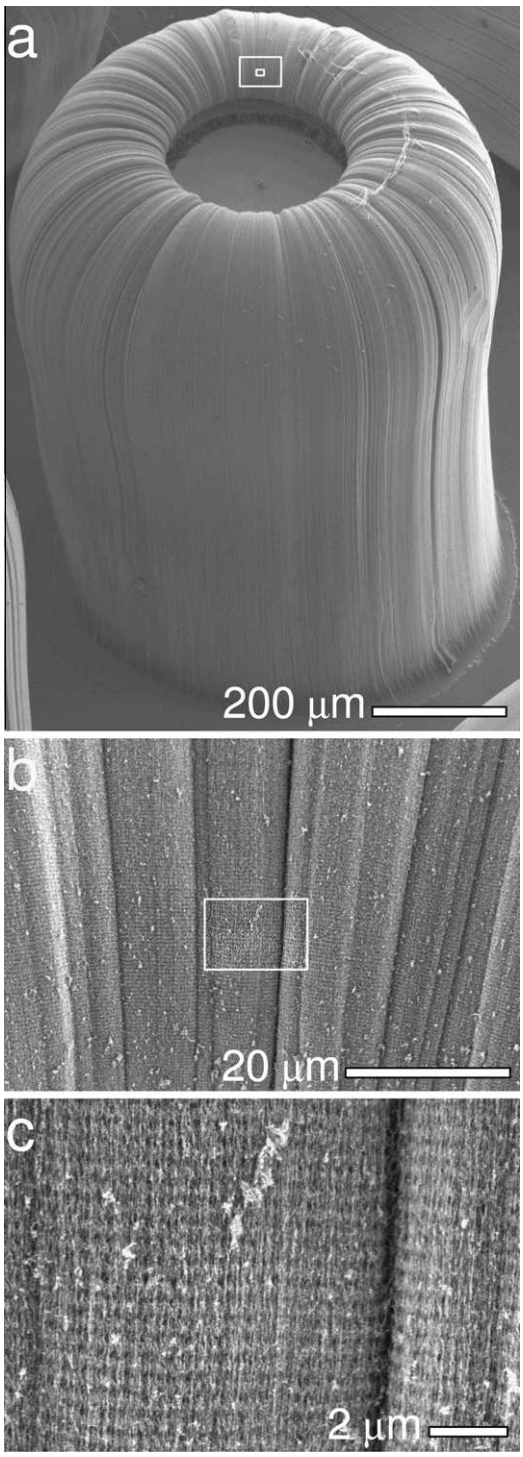

Fig. 3 – SEM images of rippled forest (700 μm diameter, ~1 mm tall). (a) Entire forest viewed at 45°. (b) Close-up image of larger box in (a) showing ripples over a wide area. (c) Close-up of box in (b). The ripple spacing is 470 ± 10 nm. This forest was grown at 760 °C using 220 sccm C_2H_2 flow rate.

that wandering nanotubes in a forest typically come into contact with one another [12,13]. While the wavelength did not vary significantly over short distances of several dozen μm on any given forest, it did vary significantly from one forest to another, even forests grown under the same conditions

or on the same growth substrate. The wavelength showed no clear trend with location on the forest.

While there are areas of several μm^2 of approximately constant wavelength and amplitude on many forests, there are occasionally abrupt changes from one wavelength and/or amplitude to another (see Fig. 1d). Such changes in wavelength are "faults" or "dislocations" in which ripples of similar wavelength become locally mismatched, as is apparent in Fig. 1c.

In situ optical monitoring during growth reveals that all the nanotubes in a forest start growing at the same time from the flat substrate (see our previous reports [12,26]). It also reveals that the top surface of the forest becomes concave as soon as the forests begin to grow, and it quickly evolves to its final form (see Fig. 1a and Fig. 3a) within a few minutes after growth is initiated (under the present growth conditions). The concave top surface must then be caused by the outer nanotubes of the forest growing faster than the inner nanotubes, clearly demonstrating the existence of a growth rate difference. This growth rate difference is well defined by the shape of the concave top surface. All rippled nanotube forests observed in the present report have concave top surfaces, which leads us to believe that, in the present case, concavity and rippling are intimately related.

Because of their small size, ripples are not directly observable using optical imaging. Previously, we showed that rippled forests, such as those in the present report, can be observed optically via diffraction because they behave as gratings [20]. This effect allows their periodicity to be directly calculated from the simple grating equation, and shows that the ripples are very consistent over significant areas, for if they were not, clear diffraction patterns, such as those observed here, would not be seen. By comparing the optically determined grating spacing with the rippling wavelength determined from SEM images of the same location on the forest as the diffraction, we correlate the diffraction to the rippled nanotubes. The fact that diffraction occurs in the visible region of the spectrum is itself an indicator that the wavelength and amplitude of the ripples are the order of magnitude as the wavelength of visible light.

In situ diffraction of white light is visible in Fig. 4a, which is a frame from video S1 (see supplementary material); a red patch of reflected light is visible on the far side of the growing forest's curved sidewalls. An SEM image of this forest is shown in Fig. 3, with the approximate location of the rippled nanotube forest grating responsible for the diffraction indicated. *Ex situ* optical examination of this forest allows the full range of angles of incidence and observation to be analyzed. Long working distance optical microscope observations of diffraction in Fig. 5 show the results from this forest in approximately the same location as seen in Fig. 4a and Fig. 3. The observed colour changes from red to blue (a–j) as the angle of incidence is swept across the sample in 4° intervals. Based on the diffraction data the grating spacing is 330 ± 140 nm, which agrees with the 470 ± 10 nm measured by SEM [20].

Iridescence was also observed *in situ* from many smaller 100 μm diameter forests growing simultaneously (see Fig. 4b and supplementary material video S2), showing that this is not an isolated phenomenon.

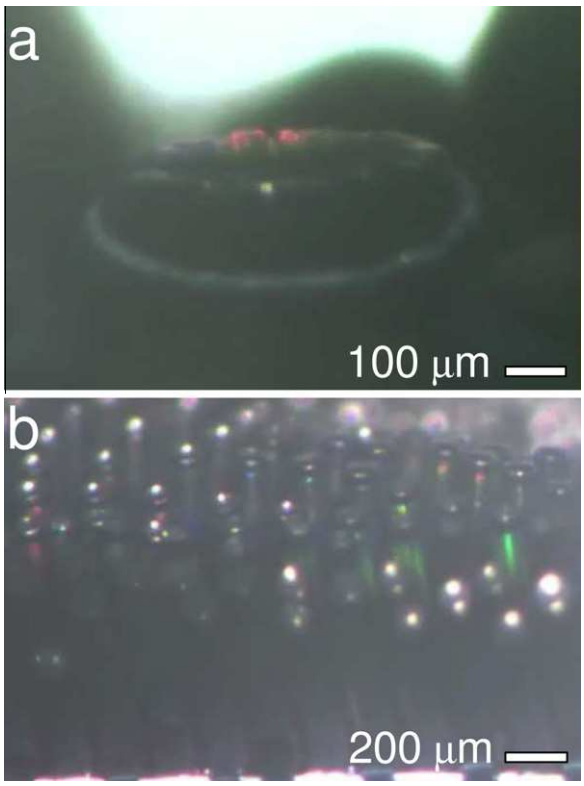

Fig. 4 – *In situ* optical images. (a) Growing 700 μm diameter forest showing iridescence (red patch) from the far side of its curved sidewalls. An SEM image of this forest is shown in Fig. 3. Iridescence occurs near the area indicated in Fig. 3. Here, the forest is observed at an ~5° glancing angle, but in the same direction as in Fig. 3. See supplementary material video S1. (b) Iridescence from multiple 100 μm diameter forests. See supplementary material video S2. Both forests were grown at 760°C using 220 sccm and 180 sccm C_2 H_2 flow rates respectively. (For interpretation of the references to colour in this figure legend, the reader is referred to the web version of this article.)

By observing the iridescence from forests as they are cooled post-growth in the reactor, we see that the diffracted colours do not change, hence the wavelength of the ripples does not change (see supplementary material video S3, which shows a sample of 100 μm diameter forests). The post-growth cooling process is therefore not involved in ripple formation. Furthermore, this shows that the ripples are remarkably stable over a wide range of temperatures. Even as the temperature is reduced from ~800 °C to room temperature (over a factor of 3 in absolute temperature) the diffracted colours, and hence the ripple wavelength, do not change at all, meaning that any thermal expansion and other relaxation effects are negligible. From *in situ* observations of iridescence, it is clear that the ripples form during the growth of the forests, and that they are minimally affected afterward.

To gain more insight into ripple formation, and because the ripples are not directly observable via optical imaging, a series of forests was grown under identical reactor conditions and intentionally halted (prior to ordinary self-termination) by stopping the flow of process gases after various growth

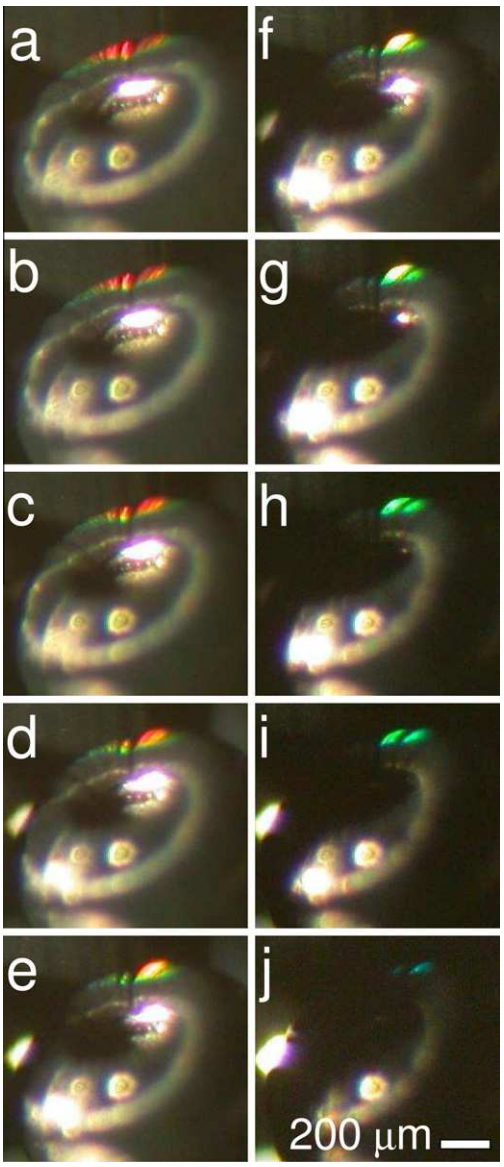

Fig. 5 – Long working distance *ex situ* optical images showing the diffraction grating effect from the forest in Fig. 3 and Fig. 4a. Colours progress from red to blue (a–j) as the angle of incidence is swept across the sample in 4° intervals. (For interpretation of the references to colour in this figure legend, the reader is referred to the web version of this article.)

times and purging the reactor with pure Ar. Subsequent *ex situ* SEM imaging of these forests reveals that ripples begin forming within the first minute, before the top surface of the forest has reached its final concave shape. On forests intentionally terminated early enough (less than 10–20 min of growth time, depending on reactor conditions), ripples are observed to extend all the way to the base of the forest. However, after longer growth times (more than 10–20 min), the rippling amplitude near the base of the forest becomes so small that ripples are not observable and the nanotubes appear straight as they near the bottom of the forest, as seen in self-terminated forests, such as Fig. 1a.

More insight into the nature and origin of these ripples comes from destructively examining a forest. By breaking open a forest with tweezers, it can be seen, using SEM, that the inner most nanotubes in the forest (those nearest the center of the circular cross section) are straight. Moving inward from the sidewalls, where the outer nanotubes are rippled with large amplitudes, toward the center, the amplitude of the ripples decreases to zero (see Fig. 2b). Thus, the rippling is not evenly distributed across the forest, unlike the random distributions in several previous reports [2,3]. The distribution observed here is different than a previously observed non-random distribution [8].

4. Discussion

Several previously published reports observe rippling as a result of *ex situ* compression [9–11]. Cao et al. [9] and Pushparaj et al. [10] see the nanotubes near the bottom of their forests buckle when an external force is applied *ex situ*. The buckling slowly disappears toward the top of the forest. They propose that this buckling is due to the compression and the spatial restrictions from neighbouring nanotubes. It is important to note that the ripples observed in these reports are not formed during the growth of the forest, but are instead formed afterward by applying an external force. Nevertheless, the visual similarities can give insight into the present data.

Hart and Slocum [1] applied external mechanical compression to forests as they grew and showed that growing nanotubes exert a force. The authors propose that the mechanical force exerted by growing nanotubes and the lateral constraint of neighbouring nanotubes forces them into their “serpentine” structure. They noted that higher applied forces produced ripples with smaller wavelengths and that the wavelength decreased toward the base of the forest. While these ripples did form during the growth of the forest, it was a result of the externally applied force.

Some reports of ripples, such as those presented here, do not involve the application of external forces, but instead have ripples that naturally form during the growth process. Rippling in specially prepared catalyst samples is observed in several reports [2–5]. Qiang Zhang et al. [2] propose that the ripples are caused by the close proximity of the nanotubes to each other and a difference in the growth rate between different nanotubes in the forest that is caused by a non-uniform catalyst nanoparticle size. They see a mixture of straight nanotubes (slow growing) and rippled nanotubes (fast growing) and note a random distribution of the rippling phenomenon. They also mention that the woven structure of nanotubes at the top of the forest causes the faster growing nanotubes to bend. Yingying Zhang et al. [3] similarly propose a difference in growth rate caused by a non-uniform catalyst nanoparticle size as the cause of the rippling. They see a random distribution of the rippled nanotubes throughout the forest, but note that it is the smaller diameter nanotubes growing from smaller catalyst nanoparticles that grow faster and are thus forced to ripple. Yongyi Zhang et al. [5] propose that their ripples are due to mechanical stresses in the forest caused by a spatial growth rate difference from an intentionally non-uniform catalyst layer.

Wang et al. [6] propose that different growth rates between nanotubes cause the faster growing tubes to adopt curved structures, both helical and zig zag. Their ripples become more prominent later in the forest growth and seem randomly distributed throughout the forest, mixed with straight nanotubes. Bedewy et al. [7] see ripples only several μm from the base of the forest, and propose that their ripples are caused by the collapse of the forest structure due to growth cessation of individual nanotubes.

Dittmer et al. [8] see a non-random distribution of ripples in their forests, though their distribution is essentially the opposite of the present report (straight nanotubes on the edges). They explain their ripples as a result of mechanical interaction between nanotubes and a non-uniform growth rate across their small forests that is in turn a result of a non-uniform temperature across their sample due to their local heating process.

The fact that ripples form during many different CVD processes, indicates that ripples are not specific to any one choice of source gas or reactor geometry.

As described above, several previous reports [2,3,5,6,8] propose that a growth rate difference was the cause of the ripples. A key difference between the present report and most of those reports [2,3,5,6] is in the distribution of the fast and slow growing nanotubes within the forest. In those reports, the distribution was random, but here the distribution is spatially non-uniform. Another report [8] saw a non-uniform growth rate distribution, but it is unlike the concentric growth rate distribution observed here.

Morphological similarities between our rippled forests and those which are generated by externally applied forces [1,9–11] suggest that strain within the forest plays a role in ripple formation.

Strain and a growth rate difference are linked together: a growth rate difference will cause the faster growing outer nanotubes to be strained by the mechanical force they exert during growth [1] against the forest above the growth front, which is held together by van der Waals interactions between nanotubes. Relative to the faster growing outer nanotubes, the forest is anchored to the substrate by the slower growing inner nanotubes. The forest and substrate then behave as top and bottom boundary conditions respectively and thus enforce a uniform vertical growth rate (equal to the slower growth rate of the inner nanotubes) upon all of the nanotubes in the forest. This top boundary condition is similar to the woven structure described by Qiang Zhang et al. [2], but is more than just a layer – it is the entire forest.

Rippling, then, is a growth instability that occurs to relieve strain. Rippling allows the faster growing outer nanotubes to grow to a longer length than the slower growing inner nanotubes in a given time interval, while still growing to the same height above the substrate in that time interval. Spatial constraints due to neighbouring nanotubes then cause the rippling [1–3,9,10] because all nanotubes are constrained to wander within a narrow region of the forest. The long range synchronization of the rippling pattern is due to the cohesive van der Waals interactions between nanotubes.

The overall forest growth would proceed as follows. When the forest begins growing, we suppose that the faster growth rate of the outer nanotubes is at first accommodated by the forest adopting the concave top surface, and later by the sidewalls curving in toward the center. This relieves strain in the process by allowing the faster growing outer nanotubes to reach their full length. As the forest gets taller it becomes increasingly rigid, and these two mechanisms cannot relieve all of the strain so the outer nanotubes begin to ripple. When the forest is sufficiently tall (when the top surface has reached its final shape) it can no longer relieve strain through increased concavity of its top surface or curving in of the sidewalls because it is too rigid. It then enforces the rigid top boundary condition over the growth front and the forest as a whole grows at a uniform rate with rippling as the sole means of strain relief. The concave top surface is therefore linked to the rippling of the sidewalls of the forests, however, it does not guarantee the presence of ripples if the growth rate difference is not sufficiently large, as described below.

As more time elapses after growth initiation, the ripples formed have progressively smaller amplitudes until the amplitude eventually reaches zero, thus terminating the rippling (see Fig. 1). We speculate that the rippling terminates because the outer nanotubes' faster growth rate decreases faster and they stop growing sooner than the inner nanotubes. This results in a decreasing growth rate difference as growth progresses, and therefore decreased mechanical strain and rippling. It has previously been shown [26,30–33] that the faster a nanotube grows (such as the outer nanotubes relative to the inner nanotubes in the present case), the sooner it stops growing. We have previously reported [12] that, under growth conditions similar to those used here, the outer nanotubes of forests have a tendency to terminate before the inner nanotubes and detach themselves from the substrate. Similarly, Bedewy et al. [7] showed (via mass density measurements of forests) that some nanotubes stop growing before the forest reaches its terminal height.

It has been shown that a non-uniform catalyst thickness can cause a growth rate difference and even cause rippling [5]. Here, we can rule this out as the cause of the growth rate difference and rippling. Edge effects are expected in the shadow mask catalyst preparation technique, and these could result in a non-uniform catalyst thickness, and therefore affect the growth rate. However, we also prepared some samples by photolithography, for which much smaller scale edge effects are expected. Both techniques resulted in the same growth rate differences and the same rippling, so we can rule out catalyst thickness variations as the cause.

For tall forests, it is sometimes speculated that the nanotubes impede the gas phase diffusion of the source gas through the forest. We can rule this out as a cause of the growth rate difference because, here, the growth rate difference exists even during the initial moments of growth when the forests are still very short. This is demonstrated by the increasing concavity of the top surface of the forest within the first minute of growth. We thus conclude that diffusion of the source gas through the forest is not the cause of the growth rate difference. This conclusion is consistent with previous reports [1,19,26,34].

A non-uniform temperature is known to cause a growth rate difference, and it has even been shown to be the cause of rippling when a sufficiently large difference is present [8]. Here, this is not the case as the heater is much larger than

the catalyst islands and non-uniformities are generally small (around ±10 °C at the most).

The most likely origin of the growth rate difference is a non-uniform local gas distribution across the catalyst island. The inner catalyst nanoparticles are surrounded by other nanoparticles consuming reactive carbon whereas the outer catalyst nanoparticles are only partially surrounded by other nanoparticles, and otherwise by non-carbon-consuming silicon dioxide. The source gas molecules impinging upon the silicon dioxide are not used for nanotube growth and thus create a larger local concentration of source gas near the edge of the forest [34]. Because the outer nanoparticles therefore receive more carbon than the inner nanoparticles, they grow faster (under the present conditions, the growth rate is limited by the carbon supply because increasing the flow rate increases the growth rate). Unlike the above diffusion through the forest being impeded by the nanotubes, this is strict gas-phase diffusion without impediment.

Given that C_2H_2 will move by gas-phase diffusion, we would expect that any variation in concentration across the catalyst/substrate boundary would have a characteristic length scale ℓ, which is expected to be on the order of the gas diffusion length (~1 μm). We expect ℓ to be independent of the size of the catalyst island. This then yields a differently shaped gas distribution across the diameter of the catalyst island for different sized islands, and hence produces the observed nanotube growth rate profile. Different growth profiles for different sized islands is possibly the reason why we see the ripples form on the 100 μm diameter forests over a wider range of conditions than the larger forests.

To estimate the magnitude of the growth rate difference involved in rippling, the rippled nanotubes on the sidewalls of the forest are assumed to be sinusoidal with amplitude 100 nm and wavelength 700 nm, as seen in Fig. 2a. Therefore, the rippled outer nanotubes are ~20% longer than the straight inner nanotubes over one period. This length difference therefore requires an ~20% faster growth rate for the outer nanotubes when compared to the inner nanotubes. This estimate is very sensitive to the amplitude/wavelength ratio. As the amplitude decreases toward the base of the forest, the growth rate difference will decrease as well. The growth conditions that lead to ripple formation are those for which a sufficiently large growth rate difference is present between different nanotubes in the forest.

The amplitude of the rippling pattern depends strongly on the growth conditions. We suppose then that variations in amplitude from one forest to another on the same growth sample are likely due to slight variations in local CVD conditions across the sample. Conversely, we see no such dependence for the wavelength, which does not generally vary much for any given forest on the several μm scale, as evidenced by the presence of clear diffraction patterns. The wavelength of the ripples likely depends primarily on the physical properties and density of the nanotubes in the forest. Variations in wavelength from one forest to another on the same sample are likely due to variations in the composition of the forests, specifically the relative numbers of different nanotubes [13] as defined by their diameter, number of walls, and crystallinity. Variations within a forest, other than abrupt changes due to "faults", are likely caused by variations in the local density of nanotubes, which is a result of nanotube wandering and the growth cessation of some individual nanotubes.

Finally, we can estimate the rippling wavelength by considering a pair of straight nanotubes interacting with each other along their length L via a van der Waals interaction. The cohesion energy of this interaction for one nanotube is $E_{co} = \epsilon_{co}\Omega^{-1}bL$, where $\epsilon_{co} \sim 25$ meV per carbon atom is the binding energy between graphene sheets [35], $\Omega \sim 0.026$ nm^2 per carbon atom is the surface density of graphene, and bL is the area of interaction (contact area) with $b \sim a = 0.14$ nm (the C–C bond length).

Using the thin rod approximation (see for example Landau and Lifshitz [36]), the bending energy is given by $E_{bend} = \frac{\pi}{8}Yr^4L/R^2$, where Y = 1 TPa is Young's modulus, r is the nanotube radius, and R is the bending radius. Setting $E_{co} = E_{bend}$ and assuming the ripple wavelength λ is on the same order of magnitude as R yields the relation:

$$\lambda \sim R = \sqrt{\frac{\pi}{8}\frac{Y\Omega}{\epsilon_{co}}\frac{r^4}{b}}$$

Importantly, this relation depends only on the properties of the nanotube itself through the radius r. If we take $r = 1$ nm, then the predicted wavelength is $\lambda \sim 140$ nm, which is on the same order of magnitude as the observations. The largest uncertainty in this estimate is the effect of the cohesion interaction (given by the contact area bL), which is manifested in the estimate for λ as $b \sim a = 0.14$ nm (the C–C bond length). Furthermore, the estimate is limited by the approximating the nanotube to be solid rod.

Because the rippling wavelength is fixed for a given type of nanotube (defined here exclusively by its radius r) according to this simple model, the rippling amplitude is a monotonic increasing function of the growth rate difference, which is in turn controlled by the reactor conditions. This agrees well with our observations that the wavelength has no clear dependence on the growth conditions, while the growth rate difference (as seen in the forest concavity) and amplitude have a maximum at the same growth conditions.

5. Conclusion

In summary, we grew vertically aligned carbon nanotube forests that had periodic ripples on their sidewalls. These ripples behave as surface diffraction gratings and allowed us to observe the ripples *in situ*. We showed that the ripples self-assemble during CVD growth of the forests under the appropriate reactor conditions, which were identified. We use this *in situ* data to support a formation mechanism: rippling occurs to relieve strain within the forest that is a result of a difference in growth rate between different nanotubes in the forest. This growth rate difference was observed using simple *in situ* optical microscopy. The order of magnitude of the rippling wavelength was predicted using a simple solid rod model for nanotubes.

Carbon nanotube forest growth is not simply the growth of many individual nanotubes: collective effects alter the way that the individual nanotubes grow within the forest. The rippling phenomenon shows that the interactions between

nanotubes in forests are indeed very important factors to consider in formulating a model for the growth of vertically aligned carbon nanotube forests. Studying and understanding the rippling is thus another step toward understanding the overall growth of nanotube forests, and eventually tailoring them to specific applications.

Acknowledgments

The authors thank the following IMS staff for their assistance and support: J. Fraser, H. Tran, M. Denhoff, and B. Lamontagne. P.V. was supported by NSERC, NRC-GSSSP and P.F.'s NSERC Discovery Grant.

Appendix A. Experimental methods

Before each growth run, the reactor was purged for 10 min with pure Ar flowing at 2 l min^{-1}. Samples were heated to the growth temperature *T* (measured with a two-colour infrared pyrometer) in an Ar/H_2 (2% H_2, 98% Ar) gas environment, with a flow rate of 170 sccm to 300 sccm, corresponding to the eventual source gas flow rate. Water vapour was then introduced by passing Ar through the bubbler to account for 25% of the total gas flow rate for 5 min while reducing the Ar/H_2 flow rate to 75% of the total gas flow rate, keeping the total gas flow rate constant. Dilute acetylene (0.1% C_2H_2, 99.9% Ar) was then introduced (90 sccm to 220 sccm) to initiate growth, while turning the Ar/H_2 and Ar/H_2O flow rates down to 60 sccm and 20 sccm, respectively, for a total gas flow rate of 170 sccm to 300 sccm. After the growth was determined to have halted via self-termination (by visual inspection with the camera), the chamber was purged for 5 min with pure Ar flowing at 2 l min^{-1}. The heater was then shut off and the Ar was allowed to flow for another 5 min before it was shut off. For forests that were intentionally terminated prior to self-termination, the process gases were stopped and the reactor was immediately purged with pure Ar. All samples remained in the Ar environment inside the reactor for at least another 30 min prior to removal to atmosphere.

Appendix B. Supplementary data

Supplementary data associated with this article can be found, in the online version, at doi:10.1016/j.carbon.2011.02.017.

REFERENCES

[1] Hart AJ, Slocum AH. Force output, control of film structure, and microscale shape transfer by carbon nanotube growth under mechanical pressure. Nano Lett 2006;6:1254–60.
[2] Zhang Q, Zhou W, Qian W, Xiang R, Huang J, Wang D, et al. Synchronous growth of vertically aligned carbon nanotubes with pristine stress in the heterogeneous catalysis process. J Phys Chem C 2007;111:14638–43.
[3] Zhang Y, Zou G, Doorn SK, Htoon H, Stan L, Hawley ME, et al. Tailoring the morphology of carbon nanotube arrays: from spinnable forests to undulating foams. ACS Nano 2009;3:2157–62.
[4] Cui X, Wei W, Harrower C, Chen W. Effect of catalyst particle interspacing on the growth of millimeter-scale carbon nanotube arrays by catalytic chemical vapor deposition. Carbon 2009;47:3441–51.
[5] Zhang Y, Gregoire JM, van Dover RB, Hart AJ. Ethanol-promoted high-yield growth of few-walled carbon nanotubes. J Phys Chem C 2010;114:6389–95.
[6] Wang H, Xu Z, Eres G. Order in vertically aligned carbon nanotube arrays. Appl Phys Lett 2006;88:213111.
[7] Bedewy M, Meshot ER, Guo H, Verploegen EA, Lu W, Hart AJ. Collective mechanism for the evolution and self-termination of vertically aligned carbon nanotube growth. J Phys Chem C 2009;113:20576–82.
[8] Dittmer S, Ek-Weis J, Nerushev OA, Campbell EEB. Growth of aligned mwnt arrays using a micrometer scale local-heater at low ambient temperature. J Nanosci Nanotech 2010;10:4015–22.
[9] Cao A, Dickrell PL, Sawyer WG, Ghasemi-Nejhad MN, Ajayan PM. Super-compressible foamlike carbon nanotube films. Science 2005;310:1307–10.
[10] Pushparaj VL, Ci L, Sreekala S, Kumar A, Kesapragada S, Gall D, et al. Effects of compressive strains on electrical conductivities of a macroscale carbon nanotube block. Appl Phys Lett 2007;91:153116.
[11] Wang BN, Bennett RD, Verploegen E, Hart AJ, Cohen RE. Characterizing the morphologies of mechanically manipulated multiwall carbon nanotube films by small-angle x-ray scattering. J Phys Chem C 2007;111:17933–40.
[12] Vinten P, Marshall P, Lefebvre J, Finnie P. Distinct termination morphologies for vertically aligned carbon nanotube forests. Nanotech 2010;21:035603.
[13] Zbib AA, Mesarovic SD, Lilleodden ET, McClain D, Jiao J, Bahr DF. The coordinated buckling of carbon nanotube turfs under uniform compression. Nanotech 2008;19:175704.
[14] Hart AJ, Slocum AH. Rapid growth and flow-mediated nucleation of millimeter-scale aligned carbon nanotube structures from a thin-film catalyst. J Phys Chem B 2006;110:8250–7.
[15] Zhang L, Li Z, Tan Y, Lolli G, Sakulchaicharoen N, Requejo FG, et al. Influence of a top crust of entangled nanotubes on the structure of vertically aligned forests of single-walled carbon nanotubes. Chem Mater 2006;18:5624–9.
[16] Hart AJ, van Laake L, Slocum AH. Desktop growth of carbon-nanotube monoliths with in situ optical imaging. Small 2007;3:772–7.
[17] Meshot ER, Hart AJ. Abrupt self-termination of vertically aligned carbon nanotube growth. Appl Phys Lett 2008;92:113107.
[18] Puretzky AA, Eres G, Rouleau CM, Ivanov IN, Geohegan DB. Real-time imaging of vertically aligned carbon nanotube array growth kinetics. Nanotech 2008;19:055605.
[19] Han JH, Graff RA, Welch B, Marsh CP, Franks R, Strano MS. A mechanochemical model of growth termination in vertical carbon nanotube forests. ACS Nano 2008;2:53–60.
[20] Vinten P, Lefebvre J, Finnie P. Visible iridescence from self-assembled periodic rippling in vertically aligned carbon nanotube forests. Appl Phys Lett 2010;97:101901.
[21] Hata K, Futaba DN, Mizuno K, Namai T, Yumura M, Iijima S. Water-assisted highly efficient synthesis of impurity-free single-walled carbon nanotubes. Science 2004;306:1362–4.
[22] Eres G, Puretzky AA, Geohegan DB, Cui H. In situ control of the catalyst efficiency in chemical vapor deposition of vertically aligned carbon nanotubes on predeposited metal catalyst films. Appl Phys Lett 2004;84:1759–61.
[23] Eres G, Kinkhabwala AA, Cui H, Geohegan DB, Puretzky AA, Lowndes DH. Molecular beam-controlled nucleation and growth of vertically aligned single-wall carbon nanotube arrays. J Phys Chem B 2005;109:16684–94.

[24] Zhang C, Pisana S, Wirth CT, Parvez A, Ducati C, Hofmann S, et al. Growth of aligned millimeter-long carbon nanotube by chemical vapor deposition. Diamond Relat Mater 2008;17:1447–51.
[25] Mattevi C, Wirth CT, Hofmann S, Blume R, Cantoro M, Ducati C, et al. In-situ x-ray photoelectron spectroscopy study of catalyst-support interactions and growth of carbon nanotube forests. J Phys Chem C 2008;112:12207–13.
[26] Vinten P, Lefebvre J, Finnie P. Kinetic critical temperature and optimized chemical vapor deposition growth of carbon nanotubes. Chem Phys Lett 2009;469:293–7.
[27] Finnie P, Bardwell J, Tsandev I, Tomlinson M, Beaulieu M, Fraser J, et al. Cold wall chemical vapor deposition of single walled carbon nanotubes. J Vac Sci Technol 2004;22:747–51.
[28] Finnie P, Li-Pook-Than A, Lefebvre J, Austing DG. Optimization of methane cold wall chemical vapor deposition for the production of single walled carbon nanotubes and devices. Carbon 2006;44:3199–206.
[29] Bajpai V, Dai L, Ohashi T. Large-scale synthesis of perpendicularly aligned helical carbon nanotubes. J Am Chem Soc 2004;126:5070–1.
[30] Picher M, Anglaret E, Arenal R, Jourdain V. Self-deactivation of single-walled carbon nanotube growth studied by in situ raman measurements. Nano Lett 2009;9:542–7.
[31] Meshot ER, Plata DL, Tawfick S, Zhang Y, Verploegen EA, Hart AJ. Engineering vertically aligned carbon nanotube growth by decoupled thermal treatment of precursor and catalyst. ACS Nano 2009;3:2477–86.
[32] Bosnick K, Dai L. Growth kinetics in a large-bore vertically aligned carbon nanotube film deposition process. J Phys Chem C 2010;114:7226–30.
[33] Picher M, Anglaret E, Jourdain V. High temperature activation and deactivation of single-walled carbon nanotube growth investigated by in situ raman measurements. Diamond Relat Mater 2010;19:581–5.
[34] Jeong GH, Olofsson N, Falk LKL, Campbell EEB. Effect of catalyst pattern geometry on the growth of vertically aligned carbon nanotube arrays. Carbon 2009;47:696–704.
[35] Schabel MC, Martins JL. Energetics of interplanar binding in graphite. Phys Rev B 1992;46:7185–8.
[36] Landau LD, Lifshitz EM. Theory of elasticity. 3rd ed. Oxford: Uk; 1986. Reed.